Protein Science (2000), *9*:265–272. Cambridge University Press. Printed in the USA.

Structure of tick anticoagulant peptide at 1.6 Å resolution complexed with bovine pancreatic trypsin inhibitor

ROBERT ST. CHARLES, K. PADMANABHAN,[1] R.V. ARNI,[2]
K.P. PADMANABHAN, AND A. TULINSKY

Department of Chemistry, Michigan State University, East Lansing, Michigan 48824-1322

(RECEIVED October 1, 1999; FINAL REVISION November 8, 1999; ACCEPTED November 19, 1999)

Abstract

The structure of tick anticoagulant peptide (TAP) has been determined by X-ray crystallography at 1.6 Å resolution complexed with bovine pancreatic trypsin inhibitor (BPTI). The TAP–BPTI crystals are tetragonal, $a = b = 46.87$, $c = 50.35$ Å, space group $P4_1$, four complexes per unit cell. The TAP molecules are highly dipolar and form an intermolecular helical array along the *c*-axis with a diameter of about 45 Å. Individual TAP units interact in a head-to-tail fashion, the positive end of one molecule associating with the distal negative end of another, and vice versa. The BPTI molecules have a uniformly distributed positively charged surface that interacts extensively through 14 hydrogen bonds and two hydrogen bonded salt bridges with the helical groove around the helical TAP chains. Comparing the structure of TAP in TAP–BPTI with TAP bound to factor Xa(Xa) suggests a massive reorganization in the N-terminal tetrapeptide and the first disulfide loop of TAP ($Cys5_T$–$Cys15_T$) upon binding to Xa. The $Tyr1_TOH$ atom of TAP moves 14.2 Å to interact with Asp189 of the S1 specificity site, $Arg3_TCZ$ moves 5.0 Å with the guanidinium group forming a cation–π-electron complex in the S4 subsite of Xa, while $Lys7_TNZ$ differs in position by 10.6 Å in TAP-BPTI and TAP-Xa, all of which indicates a different pre-Xa–bound conformation for the N-terminal of TAP in its native state. In contrast to TAP, the BPTI structure of TAP–BPTI is practically the same as all those of previously determined structures of BPTI, only arginine and lysine side-chain conformations showing significant differences.

Keywords: bovine pancreatic trypsin inhibitor; conformational changes; factor Xa; tick anticoagulant peptide

The extrinsic and intrinsic pathways of the blood coagulation cascade merge at factor Xa production, the reactions thereafter terminating in an insoluble fibrin clot. Thus, Xa plays an important pivotal role in hemostasis. With factor Va and a phospholipid surface, Xa catalyzes the Ca^{+2} ion-dependent activation of prothrombin to thrombin, which is the required enzyme in the conversion of fibrinogen to fibrin monomers. Considering the strategic position of Xa relating the coagulation pathways, inhibitors of this serine protease represent potentially useful and important antithrombotic agents.

Reprint requests to: A. Tulinsky, Department of Chemistry, Michigan State University, East Lansing, Michigan 48824-1322; e-mail: tulinsky@cem.msu.edu.

[1]Present address: Department of Biochemistry, Michigan State University, East Lansing, Michigan 48824.

[2]Present address: Department of Physics, IBILCE/UNESP, CP 136, Sao Jose do Rio Preto-SP, CEP 15054-000, Brazil.

Abbreviations: ADA, N-[2-acetamido]-2-iminodiacetic acid; amino acids of TAP and BPTI, distinguished by T or B subscript tagging residue number; BPTI, bovine pancreatic trypsin inhibitor; MALDI, matrix-assisted laser desorption ionization mass spectroscopy; P_i and S_i, peptide and enzyme site notation after Schechter and Berger (1967); TAP, tick anticoagulant peptide; TAP–BPTI, TAP–BPTI complex; TAP–Xa, TAP–Xa complex; Xa, factor Xa.

TAP is an acidic 60 residue protein produced by the soft tick *Ornithodoros moubata* and is a tenacious competitive inhibitor of Xa ($K_i = 0.59$ nM) (Waxman et al., 1990). Although its disulfide connectivity is like that of members of the Kunitz family of serine proteinase inhibitors (Fig. 1), its amino acid sequence only resembles them remotely (Antuch et al., 1994). However, NMR studies have shown that TAP possesses a generally similar, but distorted folding topology conserving a hexapeptide antiparallel β-strand and about 2.5 turns of α-helix (Antuch et al., 1994; Lim-Wilby et al., 1995). Partial structural homology notwithstanding, the N-terminal retro-binding mechanism of TAP inhibition (van de Locht et al., 1996; Wei et al., 1998), with the peptide chain running parallel to (Ser214–Gly218) of Xa, differs spectacularly from that of canonical Kunitz-type inhibitors like BPTI, where a substrate-like binding loop interacts in an antiparallel β-strand way with the active site of the enzyme (Bode & Huber, 1992). The N-terminal retro-binding mode was first observed in hirudin-thrombin (Rydel et al., 1991), and mimicked with synthetic inhibitors (Tabernero et al., 1995; Mochalkin & Tulinsky, 1999), and was also seen in the structure of the nazumamide–thrombin (Nienaber & Amparo, 1996) and the ornithodorin–thrombin (van de Locht et al., 1996) complexes, and most recently, in the crystal structure of Xa inhibited with

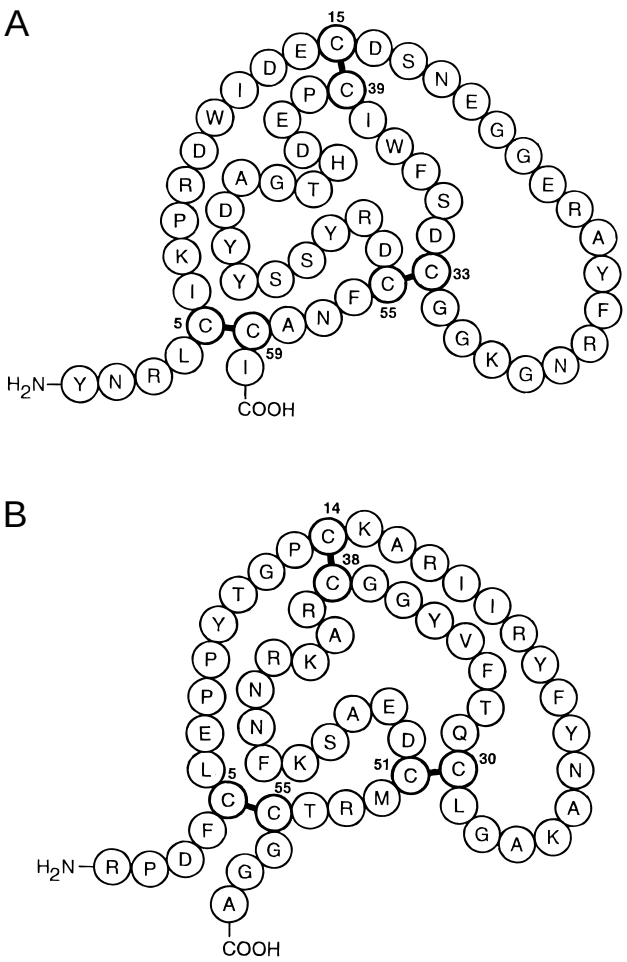

Fig. 1. Primary structures and numbering of (**A**) TAP and (**B**) BPTI.

TAP (Wei et al., 1998); in the latter, TAP showed an interaction at the active site utilizing the N-terminal $Tyr1_T$ in the S1 specificity pocket of Xa. Such binding renders TAP highly specific for Xa, which otherwise exhibits little or no appreciable inhibitory activity toward most serine proteinases including trypsin, thrombin, and other blood proteases (Waxman et al., 1990). Other elements of the TAP structure, including some of the C-terminal α-helix, are involved in Xa binding through a secondary binding site near the Na^+ ion binding site of Xa (Zhang & Tulinsky, 1997) in support of a two-step binding mechanism proposed on the basis of mutagenesis (Jordan et al., 1992).

We present here a high resolution (1.6 Å) crystal structure of TAP cocrystallized with BPTI. The new model of the TAP structure clarifies portions of the molecule that were poorly defined in previous work. Considerable differences in structure exist in the N-terminal 15 residues between TAP bound to Xa and TAP in the TAP–BPTI complex, indicating a different pre-Xa–bound conformation for the N-terminal peptide in its native state and a possible means for rationalizing the two step binding mechanism of TAP to Xa (Jordan et al., 1992; Wei et al., 1998). Crystal lattice interactions are responsible for an unusual intermolecular helical packing arrangement of TAP molecules along the crystallographic *c*-axis, with the negatively charged helical TAP groove being filled by positively charged BPTI molecules.

Results and discussion

Electron density for both TAP and BPTI was well defined in the final $(2F_o - F_c)$ map, allowing all the residues in both molecules to be modeled. Density was weaker for the last two of BPTI ($Gly57_B$–$Ala58_B$) suggesting some flexibility at the C-terminus ($\langle B \rangle \sim 30$ Å^2 compared to average values of 18.5 Å^2 for TAP and 22.8 Å^2 for BPTI). Both termini of TAP, however, were exceptionally well defined. Difference $(F_o - F_c)$ density maps were used to additionally assign 120 solvent water molecules and three clearly defined and resolved sulfate anions. The latter interact multiply and electrostatically, compensating charge through ion pairs and/or forming hydrogen bonds with nearby proton donors of arginine, lysine, or tyrosyl side chains of TAP, BPTI, and neighboring water molecules (Table 1). The first sulfate makes an ion pair with $Arg42_B$, the second with $Lys15_B$ and $Arg17_B$ of symmetry related BPTI molecules, and the last with $Arg20_B$ and $Lys30_T$. It is noteworthy that $Lys15_B$ is the P1 specificity residue of BPTI when complexed with trypsin (Bode & Huber, 1992).

The TAP–BPTI structure

Attempts to grow crystals of TAP from solutions of the homogenous protein proved to be unsuccessful. Because the isoelectric point of TAP is 4.65 while that of BPTI is 9.24, an attempt was made to cocrystallize an equimolar solution of the two reasoning that the basic regions of BPTI might electrostatically complement electronegative ones of TAP and thus facilitate crystallization of a complex. It was, therefore, reassuring when MALDI mass spectrometric analysis confirmed the composition of crystals as containing both TAP and BPTI. Other relevant factors considered were: (1) the molecules were expected to be similar in molecular size, and (2) possibly similar in structure by virtue of their near

Table 1. *Hydrogen-bonded and hydrogen-bonded ion pair interactions of sulfate anions in TAP–BPTI*

			d (Å)
SO_4–1	O-1	$N2_TND2$	3.01
	O-1	$Y49_TOH$	3.19
	O-1	O_W161	3.12
	O-2	$R42_BN$	2.79
	O-2	$R42_BNE$	3.00
	O-3	O_W253	2.86
	O-4	$R42_BNH2$	2.75
	O-4	O_W279	2.58
SO_4–2	O-2	$K15_BNZ$	2.58[a]
	O-2	$R17_BNH2$	3.40[b]
	O-3	$R17_BNE$	3.12
	O-3	O_W254	2.88
	O-4	$R17_BN$	2.80
	O-4	O_W217	2.94
SO_4–3	O-1	$K30_TNZ$	3.88[b]
	O-2	$R20_BNH2$	2.76
	O-3	$Y35_BOH$	2.83
	O-4	$R20_BNH1$	3.10

[a] From a symmetry-related BPTI molecule.
[b] Ion pair interaction only?

identical disulfide connectivity even though there is no significant level of sequence homology between the two (Fig. 1) (Antuch et al., 1994). NMR structure determinations of TAP (Antuch et al., 1994; Lim-Wilby et al., 1995) and the crystal structure of TAP-Xa (Wei et al., 1998) showed that only a two-chain β-strand and a C-terminal helix superposed on the structure of BPTI ($Glu22_T$–$Arg27_T$, $Cys33_T$–$Ile38_T$, and $Tyr52_T$–$Cys59_T$, respectively, in the present case), although other comparably sized regions are superposable separately.

The crystal structure of TAP-BPTI consists of one TAP molecule and one BPTI molecule in the asymmetric unit, with a protein fraction of 60% corresponding to a tight packing arrangement consistent with the strong X-ray diffraction characteristics of the crystals (better than 1.6 Å resolution; $I/\sigma(I) \sim 4.0$ at 1.6 Å, Table 2). Based on the crystal structure, there is no single dominant surface interface between the two molecules to suggest they crystallized from solution as a hetero-dimeric complex. Instead, the TAP and BPTI molecules appear to have added to the growing TAP–BPTI crystal independently as monomers. The TAP molecules are highly dipolar (Figs. 2, 3), and form an intermolecular helical array along the *c*-axis of the crystal with a diameter of ~45 Å (Fig. 4) satisfying 4_1 crystallographic screw axis symmetry and making 42 contacts less than 3.6 Å between TAP molecules. They interact in a head-to-tail fashion, with the electropositive end of one molecule containing the *N*- and *C*-termini (Figs. 2, 3) associating with the distal electronegative end of another, and vice versa (Fig. 4). BPTI molecules are inclined to the helix axis and interact with the helical groove around the intermolecular TAP chains through seven molecules, making a total of 57 contacts less than 3.6 Å per TAP module, two of which are hydrogen-bonded salt bridges from different BPTI units ($Arg3_T$, $Asp3_B$, and $Asp16_T$, $Arg17_B$) along with 14 other hydrogen bonds (Table 3). The TAP helix is principally held together by two hydrogen-bonded salt bridges ($Tyr1_T$, $Glu22_T$, and its reciprocal) along with four hydrogen bonds (and their reciprocals). In addition, there are 18 contacts less than 3.6 Å, and a salt bridge ($Asp13_T$, $Arg23_T$) between separate TAP helices, while BPTI molecules also interact with each other only sparingly (18 contacts less than 3.6 Å, including reciprocals) four of which are between BPTI molecules intercalated in different TAP helices (Table 3).

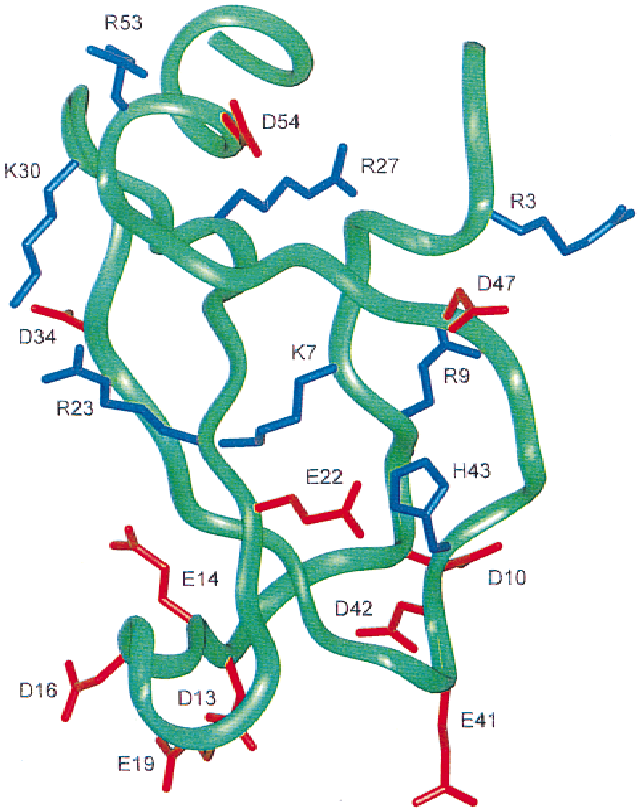

Fig. 2. Ribbon drawing of TAP indicating the locations and orientations of charged side chains. Negative groups in red, positive in blue, both numbered.

Table 2. *Diffraction data and refinement summary statistics*

Resolution (Å)	1.62
Observations ($I/\sigma(I) > 1.0$)	86,488
$I/\sigma(I)$ (outermost range) (1.88–1.62) Å	3.9
Independent reflections	13,056
Redundancy	6.6
Completeness (%)	93.1
Outermost range (%)	88.4
R_{merge} (%)	5.4
Outermost range (%)	18.8
Protein atoms	943
Water molecules	120
Refinement range (Å)	8.0–1.62
Number reflections	12,942
R_{final} (%)	18.8
R_{free} (%)	21.1
RMSΔs from ideal values	
Bond lengths (Å)	0.011
Bond angles (deg)	1.49
$B_{main\ chain}$ (Å^2)	1.8
$B_{side\ chain}$ (Å^2)	3.1

The structure of TAP in TAP–BPTI and TAP–Xa

The TAP structure of TAP–BPTI is only remotely similar to that of two NMR structure determinations [Protein Data Bank (PDB) code: 1TAP (Antuch et al., 1994) and 1TCP (Lim-Wilby et al., 1995)], but resembles that of TAP in the crystal structure of the TAP–Xa complex [PDB code: KIG (Wei et al., 1998)] fairly closely. Of the sets of NMR solutions of 1TAP and 1TCP, the smallest RMS difference between optimally superposed CA positions on TAP of TAP–BPTI (60 CA) was found to be 1.7 Å (1TAP, model 19). Compared with the NMR structures, the TAP from the TAP–Xa crystal structure is more like that of TAP–BPTI, giving an RMS difference between superposed models of 1.4 Å (60 CA positions), but 0.64 Å when using 50 selected CA positions. Although a crystallographic BPTI structure [PDB code: 4PTI (Marquart et al., 1983)] led to the molecular replacement location of BPTI in TAP–BPTI, the NMR models failed to fix the position of TAP, whereas TAP of TAP–Xa led to a satisfactory molecular replacement solution. The largest differences in structure found between TAP–BPTI and TAP–Xa are within the N-terminal segment, principally between $Tyr1_T$ and $Cys15_T$, and in the ($Asn28_T$–$Gly31_T$) loop. Significant variation within these regions is also observed between the

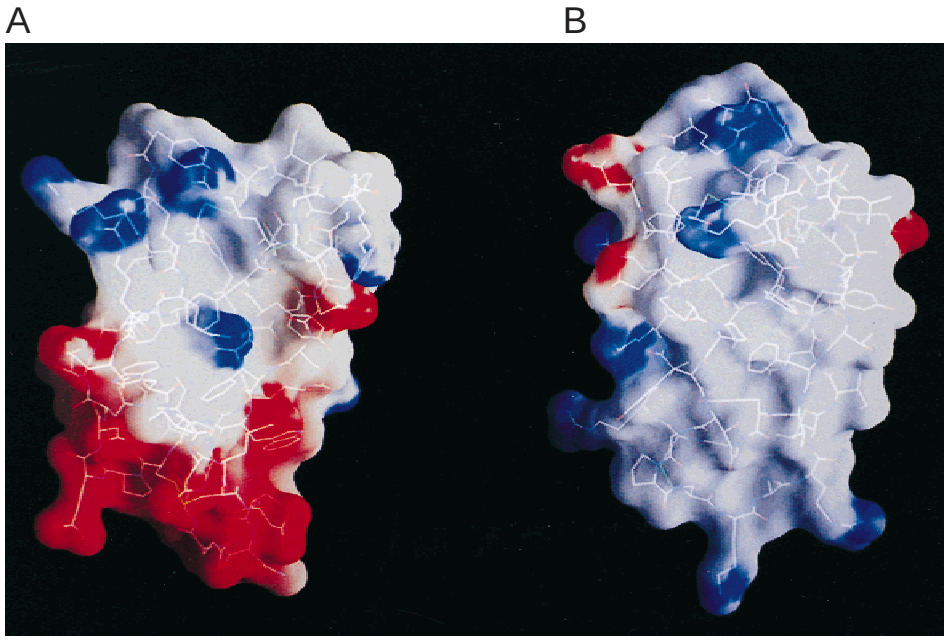

Fig. 3. Electrostatic potential surface of (**A**) TAP and (**B**) BPTI calculated using the program GRASP (Nicholls et al., 1991). ESP > 10 kT, blue; < −8 kT, red; ~0, gray.

NMR structures, suggesting that the segments are inherently flexible in TAP.

The N-terminal tripeptide of TAP binds to the active site of Xa (Wei et al., 1998) in a retro-manner (Tabernero et al., 1995; Nienaber & Amparo, 1996; van de Locht et al., 1996; Mochalkin & Tulinsky, 1999) with the peptide chain running parallel to (Ser214–Gly218) of Xa, not unlike the N-terminal residues of hirudin in the hirudin–thrombin complex (Rydel et al., 1991). Although the

Table 3. *Intermolecular hydrogen bonds in TAP–BPTI crystals*

TAP	TAP	*d* (Å)	TAP	BPTI	*d* (Å)	BPTI	BPTI	*d* (Å)
Tyr1N	Glu22OE1	2.89[a]	Arg3NH1	Asp3OD1	3.10[a]	Leu6O	Gly57O	3.01
Tyr1N	Glu22OE2	3.07[a]	Arg3NH1	Asp3OD2	2.81[a]	Glu7OE1	Ala58O_T[d]	3.18
Asp13OD1	Arg23NH1	3.40[a,b,c]	Arg3NH2	Asp3OD2	2.45[a]	Pro13O	Arg17NH1	2.68[b]
Asp13OD1	Arg23NH2	2.94[a,b]	Arg9NE	Ala27O	3.22			
Asp13OD2	Arg23NH1	3.14[a,b]	Asp16OD1	Arg17NH1	3.59[a,c]			
Arg27NH1	Pro40O	2.91	Asp16OD1	Arg17NH2	3.08[a]			
Arg27NH1	His43O	2.97	Asp16OD2	Arg17NH1	2.72[a]			
Arg27NH2	His43O	3.10	Asn18ND2	Cys14O	2.96			
Gly29O	Arg53NH2	2.40[b]	Asn18ND2	Ala16O	2.89			
Gly29O	Arg53NH1	3.00[b]	Tyr25OH	Glu49OE1	2.56			
Gly31N	Glu41OE1	2.79	Asn28ND2	Asp50OD2	3.21			
			Gly31O	Arg53NH2	3.16			
			Asp34OD1	Ser47OG	2.74			
			Asp47OD2	Asp3N	2.68			
			Asp47O	Arg42NH1	3.16			
			Asp47O	Arg42NH2	3.03			
			Tyr52OH	Arg53NE	3.03			
			Tyr52OH	Asp50OD1	2.68			
			Ile60O	Arg39NH2	3.01			
			Ile60O	Arg39NH1	3.03			

[a]Hydrogen-bonded salt bridge.
[b]Between TAP helices.
[c]Might simply be a nonhydrogen-bonded salt bridge.
[d]Terminal carboxylate oxygen.

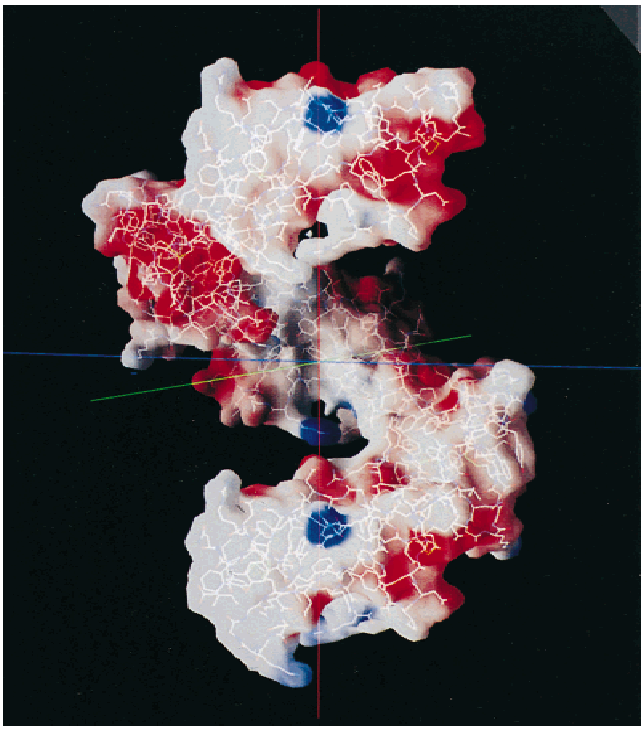

Fig. 4. Electrostatic potential surface of the intermolecular TAP helix of TAP-BPTI. Calculated using the program GRASP (Nicholls et al., 1991). ESP $>$ 10 kT, blue; $<$ −8 kT, red; ∼0, gray. Five TAP molecules of helical array shown.

(Asn2$_T$–Arg3$_T$) residues of TAP–BPTI possess a nearly ideal extended backbone conformation similar to that found in TAP–Xa, the side chains of Tyr1$_T$ and Arg3$_T$ of the two structures are severely rotated with respect to each other (Fig. 5): Tyr1$_T$OH swings 14.2 Å to bind with Asp189 in the S1 specificity site while the guanidino group of Arg3$_T$ moves to form a cation–π-electron complex in the S4 subsite of Xa (Dougherty & Stauffer, 1990; Schwabacher et al., 1993; Lin & Johnson, 1995). Both of these residues have been shown to be crucial for inhibitory activity. The site specific mutation of R3N leads to a 40,000-fold decrease in activity, while removal of Tyr1$_T$ produces a 1,000-fold loss (Dunwiddie et al., 1992). The tyrosyl group of Tyr1$_T$ in TAP–BPTI packs against the (Cys5$_T$–Cys59$_T$) disulfide bridge with its hydroxyl making intramolecular hydrogen bonds with Cys59$_T$O (2.80 Å) and the guanidinium group of Arg27$_T$NH1 (3.13 Å) (Fig. 5). The latter residue is also involved in hydrogen bonds between TAP molecules within a TAP helix (Table 3). Although Tyr1$_T$N makes a salt bridge with Glu22$_T$ in the TAP helix (Table 3), the conformation of the residue appears to be the natural one of the native state by virtue of its association with (Cys5$_T$–Cys59$_T$) and Arg27$_T$, and the fact that no further movement is necessary to form the intermolecular salt bridge: Tyr1$_T$N is already positioned optimally for the interaction in this conformation. The conformation of the Tyr1$_T$ tyrosyl is, moreover, similar to that of the CA–CD atoms of Arg1$_B$, which also interact with the (Cys5$_B$–Cys55$_B$) disulfide of BPTI like the tyrosyl of TAP.

The extended (Asn2$_T$–Arg3$_T$) dipeptide is part of a 3_{10} turn arrangement involving (Asn2$_T$–Leu4$_T$), with a hydrogen bond between Asn2$_T$O and Cys5$_T$N. In one of the NMR ensembles (An-

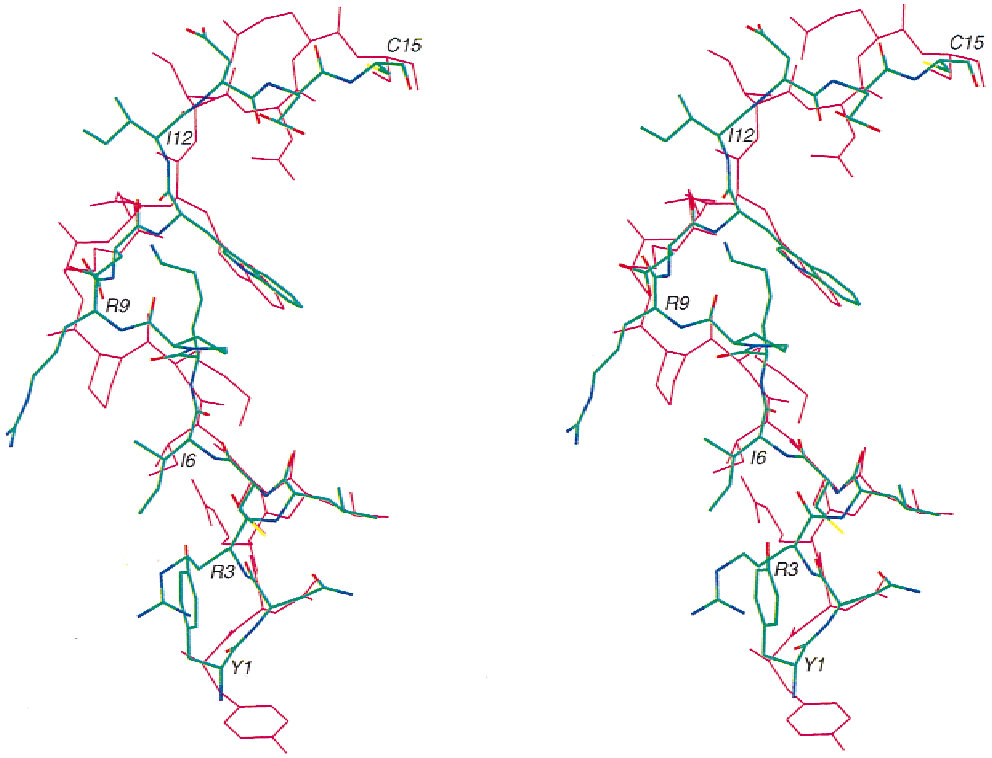

Fig. 5. Stereoview of the superposition of Tyr$_T$1–Cys$_T$15 of TAP in TAP–BPTI on TAP in TAP–Xa. TAP of TAP-BPTI in atom colors: carbon, green; nitrogen, blue; oxygen, red; sulfur, yellow. TAP of TAP–Xa in magenta. Numbering provided as a guide (residues 6 and 12 are Ile).

tuch et al., 1994), the N-terminal region is disordered, while the other (Lim-Wilby et al., 1995) is consistent with a 3_{10} helix similar to that found in TAP–BPTI and TAP–Xa. A corresponding 3_{10} structure also occurs at the N-terminus of BPTI. The N-terminal tyrosyl orientation in TAP–BPTI most likely represents a stable pre-Xa–bound conformation that changes to the more extended one when TAP interacts with the active site of Xa burying the $Tyr1_T$ side group in the S1 specificity pocket (Wei et al., 1998). Crystal packing interactions could be partially responsible for the tyrosyl position in TAP–BPTI, as this region associates somewhat with a cavity of a symmetry-related TAP molecule. However, presence of the 3_{10} turn in NMR solution structures, the similarity of the conformations of the side groups of $Tyr1_T$ and $Arg1_B$, their intramolecular disulfide associations in both TAP and BPTI, and the hydrogen bond to $Arg27_T$ in TAP, all rule against the possibility.

Comparing the TAP structure of TAP–BPTI with that of TAP in TAP–Xa suggests that $Asn2_T$ may play a more significant role in the binding of TAP to Xa than initially thought. In addition to hydrogen bonds between $Asn2_T$ (N and OD1) and the active site of Xa (Gln192OE1 and Gly218N, respectively) (Wei et al., 1998), $Asn2_T$ND2 makes another obviously important intramolecular hydrogen bond with $Tyr49_T$OH (2.86 Å). This interaction helps to further fix and maintain the position of the (Asn2–Leu4) 3_{10}-turn. In TAP–BPTI, the $Tyr49_T$ hydrogen bond is mediated by SO_4–1 (Table 1), is a little longer (3.13 Å), and not as linear. Nonetheless, its presence in TAP–BPTI stabilizes the position of the 3_{10}-turn close to the optimal one found in the TAP–Xa bound structure: a small shift in the $Asn2_T$ side group on binding to Xa leads to a geometrically ideal ($Asn2_T$ND2–$Tyr49_T$OH) hydrogen bond (distance and angle) at the expense of losing the sulfate ion interaction and slightly disrupting the better-defined 3_{10}-turn hydrogen bond of TAP–BPTI. Although the energetic trade-off on Xa binding appears to be about equally compensated, the importance of the entropic contribution of TAP in the TAP–BPTI structure is to be noted, maintaining the proper position of the 3_{10}-turn for binding to Xa. The key residue overseeing this role is $Asn2_T$. A similar stabilization of the N-terminal 3_{10}-turn in BPTI also occurs, but through a nonpolar hydrophobic interaction between $Pro2_B$ and the ($Cys5_B$–$Cys59_B$) disulfide bridge.

In addition to the changes of the N-terminal tetrapeptide, considerable variation in the structure of the first disulfide loop of TAP ($Cys5_T$–$Cys15_T$) is also observed between TAP in TAP–BPTI and the Xa bound structure that could be the result of a massive reorganization of the region accompanying binding to Xa (Fig. 5). The largest deviations are within the $Lys7_T$ to $Asp10_T$ segment. The lysyl group of $Lys7_T$ is somewhat important in the Xa complex, binding indirectly with the cation hole (Brandstetter et al., 1996; Mochalkin & Tulinsky, 1999) of the S4 subsite (hydrogen bonded salt bridge, $Lys7_T$NZ–Glu97OE2, 3.00 Å), where the guanidinium group of $Arg3_T$ also forms a cation–π-electron complex with Tyr99, Phe174, Trp215, and a hydrogen-bonded salt bridge with the other cation hole carboxylate oxygen of Glu97OE1 (Wei et al., 1998). The NZ atoms of $Lys7_T$ in TAP–BPTI and TAP–Xa differ in position by 10.6 Å, while $Arg3_T$CZ differs by 5.0 Å on binding to the S4 site. Optimal superposition of $Ty1_T$–$Ile6_T$ of TAP–BPTI and TAP–Xa shows that the χ values of CB and CG of $Arg3_T$ are similar, while those of the remaining atoms differ. Because $Arg3_T$ is a surface residue (Figs. 2, 3), its terminal atoms appear to be in different positions in the two structures due to Xa binding in TAP–Xa and salt bridge formation between $Arg3_T$ and $Asp3_B$ in TAP-BPTI (Table 3), so its native conformation remains uncertain.

The differences in structure of the first disulfide loop of TAP in TAP–BPTI and TAP–Xa start at the $Ile6_T$ side group and are followed by those of $Lys7_T$, with the two lysyl groups projecting in opposite directions (Fig. 5). The $Pro8_T$ residue in TAP–BPTI partially overlaps the lysyl position in the TAP–Xa complex while its ($Pro8_T$–$Trp11_T$) segment exhibits a type 1 β-bend, with the proline ring and the indole of $Trp11_T$ stacking on one another. The position of $Pro8_T$ is displaced by a residue in TAP–Xa, while the side groups of $Arg9_T$ and $Asp10_T$ are completely different, as are the orientations of the indole rings of $Trp11_T$ (Fig. 5). The differences then continue on to the disulfide bridge at $Cys15_T$. Although some of the smaller changes in structure could be due to crystal packing interactions, in either the TAP–BPTI or TAP–Xa crystals, the main-chain differences and the large side-group re-orientations between the two must be considered conformational changes accompanying TAP binding to Xa.

The largest differences in structure between TAP–BPTI and TAP–Xa are essentially all confined to the first 15 residues of TAP. Other lesser differences are: (1) in a small surface loop ($Asn28_T$–$Gly31_T$), due to a peptide flip between ($Asn28_T$–$Gly29_T$), (2) another peptide flip at $Asp34_T$, (3) the side chain of $Glu41_T$, (4) the orientation of the imidazole ring of $His43_T$, (5) the χ_1 angle of $Asp47_T$, and (6) some differences in the C-terminal helix; differences (3) and (4) could be due to formation of intermolecular hydrogen bonds within the TAP helix (Table 3). The TAP molecule has a secondary binding site on Xa (Wei et al., 1998). Of the six TAP residues that bind to the site, four display a high degree of structural fidelity compared to TAP-BPTI (including all the main-chain interactions), whereas the side groups of $Asp47_T$ [(5) above] and $Tyr49_T$ are different. The $Asp47_T$ residue is involved in three hydrogen bonds with BPTI in TAP–BPTI (Table 3) so that the different position of the $Asp47_T$ side chain in TAP–Xa appears to be due to Xa binding and the formation of a salt bridge with Arg222 and Lys224 of the secondary binding site. The latter residues are not only constituents of this additional Xa binding site but are also residues of the Na^+ ion binding site of Xa (Zhang & Tulinsky, 1997). The relationship between the two sites, however, could not be correlated further because the Na^+ ion and water structure of the TAP–Xa complex was not reported. Finally, the $Tyr49_T$ shift leads to a hydrogen bond with Glu146 of the Xa secondary site, and in addition, improves the one to $Asn2_T$ND2 of the N-terminal of TAP; the latter helps maintain the position of the ($Asn2_T$–$Leu4_T$) 3_{10} turn already mentioned in the TAP–Xa complex.

The general conservation of the conformation of TAP residues that interact with the secondary binding site of Xa in the two-step TAP–Xa binding mechanism (Jordan et al., 1992) suggests that the initial and rapid kinetic step in the binding of TAP to Xa most likely involves binding to the secondary site (Wei et al., 1998). The large conformational changes in the TAP N-terminus are then probably responsible for the slower, tight-binding step. Thus, the TAP–BPTI structure provides additional pertinent evidence regarding the TAP–Xa binding mechanism, clearly indicating the conformational changes that occur in TAP.

The structure of BPTI

The structure of BPTI in TAP–BPTI crystals is practically the same as that of previously determined crystal structures of BPTI (Marquart et al., 1983; Wlodawer et al., 1987a, 1987b; Lubkowski & Wlodawer, 1999). When compared with the 4PTI coordinates (Marquart et al., 1983), optimal superposition of all CA atoms,

except that of the C-terminal Ala58 residue, gives an RMS difference of 0.40 Å. Significantly, however, the side chains of 6 of the 10 arginine/lysine residues of BPTI in TAP–BPTI have different orientations. Three of the differences are most likely due to TAP–BPTI interactions ($Arg17_B$, $Arg42_B$, $Arg53_B$; Table 3). Another outstanding difference is in the $Glu7_B$ side chain that makes a hydrogen bond with the carboxylic terminal of $Ala58_B$ of a symmetry-related BPTI molecule (Table 3). This difference is most likely due to the presence of SO_4–1 in TAP–BPTI, which partially occludes the same region occupied by the side group of $Glu7_B$ of the BPTI structure.

Materials and methods

The TAP used for crystallization was recombinant material provided by Corvas International, Inc. (San Diego, California) (Lim-Wilby et al., 1995); the BPTI was purchased from Calbiochem (La Jolla, California). Using a cocrystallization approach, crystals of a 1:1 complex of TAP–BPTI were successfully grown by the vapor diffusion hanging drop method. The protein solution was prepared by first combining equal proportions of 20 mg/mL solutions of each protein and then allowing them to stand overnight at 4 °C. Crystallization drops were made by mixing 2 μL of the protein solution with an equal volume of well solution consisting of 0.1 M ADA buffer, pH 6.5, 1.2 M ammonium sulfate. Elongated crystals grew in about seven days that belong to the tetragonal system, space group $P4_1$ or $P4_3$, with unit cell dimensions $a = b = 46.87$ and $c = 50.35$ Å. MALDI mass spectrometric analysis confirmed the composition of the crystals as containing both TAP and BPTI. Four TAP–BPTI complexes per unit cell (one per asymmetric unit) give $V_m = 2.06$ Å^3/Da and a protein fraction = 0.60.

An unusual and somewhat interesting phenomenon was observed in growing TAP–BPTI crystals. When seeded with a BPTI single crystal, TAP–BPTI crystals grew in roughly concentric circles around the seed, pointing in generally radial directions at the seed (Fig. 6). Although only an apparent curiosity, it may be related to the highly dipolar nature of TAP–BPTI crystals arising from the macroscopic dipole expected of the TAP helices in crystals (Fig. 4), which originates from the electrostatic compensation of markedly dipolar TAP molecules (Figs. 2, 3) over a relatively large distance but leaves opposite electrostatic charges uncompensated at either end of the helix.

X-ray diffraction intensity data of a TAP–BPTI crystal were measured using a RAXIS-II image plate detector mounted on an Rigaku RU200 rotating anode X-ray generator producing CuK_α radiation with a graphite monochrometer at 50 kV/100 mA power. A TAP–BPTI crystal (0.6 × 0.4 × 0.2 mm) sealed in a glass capillary diffracted X-rays to better than 1.6 Å resolution at room temperature [$I/\sigma(I) \sim 4.0$ in the outermost range]. Two and a half degree oscillation frames were measured at a crystal-detector distance of 60 mm and swing angle of 0°, thus sweeping out diffraction data to a maximum resolution of 1.6 Å. A total number of 72 frames of diffraction data were recorded. The raw intensities were reduced to scaled structure amplitudes using the R-AXIS data processing software package (Higashi, 1990), results of which are summarized in Table 2.

The crystal structure of TAP–BPTI was solved by molecular replacement using the program AMoRe (Navaza, 1994) from the CCP4 crystallographic package (Laskowski et al., 1993). An initial self-rotation search to check for symmetry between TAP and BPTI did not produce any significant peaks in agreement with lack of sequence and structure homology (Antuch et al., 1994). A rotation-translation search for BPTI was then performed using the coordinates of a previously determined BPTI crystal structure (PDB code: 4PTI) (Marquart et al., 1983). The search was carried out using the (8.0–2.5) Å data and a 15 Å radius of integration. A translation search of the most outstanding rotation result produced a single unambiguous solution in space group $P4_1$ with a correlation coefficient of 0.37 and R_{factor} of 51.8%. A similar solution was found using the 8.0–3.0 Å and 8.0–2.0 Å data but was not produced using the 8.0–3.5 Å resolution range. Rigid body refinement of the 8.0–2.5 Å solution resulted in a correlation of 0.44 and an R_{factor} of 50.1%.

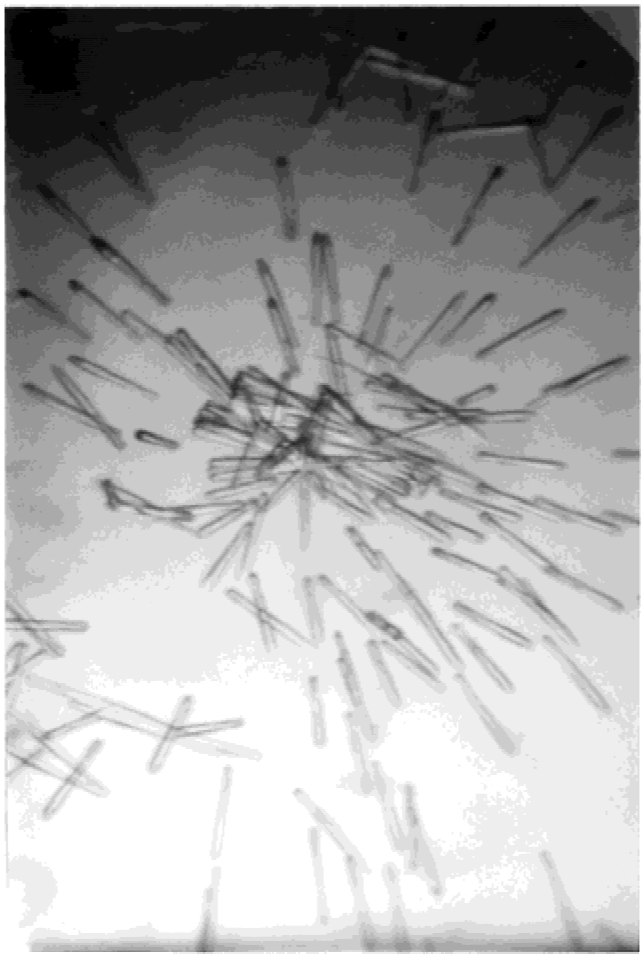

Fig. 6. Crystals of TAP–BPTI in a 10 μL sitting drop. Central crystal is a BPTI seed crystal.

With the BPTI molecule fixed, a rotation and translation search was carried out based on TAP models derived from two separate NMR structure determinations [PDB code: 1TAP (Antuch et al., 1994) and 1TCP (Lim-Wilby et al., 1995)]. These searches did not produce any significant solutions. Electron density maps using phases based on BPTI alone did not show continuous density of a TAP molecule and were difficult to interpret due to many breaks in the density. Although small segments of polyalanine peptides, presumably corresponding to TAP structure, were introduced into calculations that refined to $R \sim 30\%$ at 2.8 Å resolution, the density was still generally uninterpretable in terms of a TAP molecule.

However, using the TAP coordinates of the recently released crystal structure of the TAP–Xa complex (PDB code: 1KIG) (Wei et al., 1998) proved otherwise. A single solution in the 8.0–2.5 Å range was found using this TAP coordinate set as a search model even though it ranked 18th in the rotation solution list (correlation 0.54, R_{factor} = 45%). Using a modified model of TAP in which the first four N-terminal residues ($Tyr1_T$–$Leu4_T$), which bind to the active site of Xa (Wei et al., 1998), and the C-terminal $Ile60_T$ were omitted, along with 10 arginine and lysine side chains beyond the CB atom, the same rotation solution was obtained, but now ranked first in the rotation list. Concurrent rigid-body refinement of the TAP and BPTI models produced a correlation of 0.59 and an R_{factor} of 44.2%.

Positional and thermal parameter refinement of the TAP–BPTI model was conducted using the program CNS (Brünger, 1998). An initial simulated annealing refinement of the complex was carried out with (8.0–2.0) Å data using the slow-cool procedure in which the temperature was decreased from 2,000 to 300 K in 25° intervals. In this and all subsequent refinements, about 5% of the data set (665 reflections) was withheld for calculating the R_{free} value. The slow-cool procedure reduced the R_{factor} from 46.7% (R_{free} = 47.0%) to 32.4% (R_{free} = 40.1%). This was followed by 100 cycles of conjugate gradient positional refinement and 30 cycles of individual isotropic *B* refinement concluding at R = 30.4% (R_{free} = 38.8%). The corresponding $(2F_o - F_c)$ electron density map revealed excellent density for both molecules, most of BPTI and about 3/4 of TAP. Manual rebuilding was required to properly fit the differently positioned first loop segment of TAP ($Tyr1_T$–$Cys15_T$) and a smaller loop ($Asn28_T$–$Gly31_T$) compared to the TAP–Xa structure. Extending resolution to 1.6 Å, the TAP–BPTI model was improved further through several more rounds of manual adjustment and positional refinement (200 cycles). During this stage, solvent molecules and three sulfate ions were fitted to the difference electron density maps. The final round of positional and individual isotropic B_{factor} refinement in the 8.0–1.6 Å resolution range including occupancies of water molecules produced an *R*-value of 18.8% (R_{free} = 21.1%). The Ramachandran ϕ/ψ values of both proteins all fall within energetically allowed regions. The occupancies of the water molecules are all >0.62 with $\langle B \rangle$ = 34 Å^2. The $\langle B \rangle$ value of TAP is 18.5 Å^2, whereas that of BPTI is 22.8 Å^2. A summary of refinement statistics is given in Table 2. The coordinates of TAP–BPTI have been deposited in the PDB code 1D0D.

Acknowledgments

This work has been supported by NIH Grants HL25942 and HL43229. We also thank Corvas International, Inc. for partial financial support and providing samples of recombinant TAP, and Terry Brunck for numerous discussions throughout the course of this work.

References

Antuch W, Guntert P, Billeter M, Hawthorne T, Grossenbacher H, Wuthrich K. 1994. NMR solution structure of the recombinant tick anticoagulant protein (rTAP), a factor Xa inhibitor from the tick *Ornithodoros moubata*. *FEBS Lett 352*:251–257.

Bode W, Huber R. 1992. Natural protein proteinase inhibitors and their interaction with proteinases. *Eur J Biochem 204*:433–451.

Brandstetter H, Kuhns A, Bode W, Huber R, van der Saal W, Withersohn K, Engh RA. 1996. X-ray structure of active site-inhibited clotting factor Xa. *J Biol Chem 271*:29988–29992.

Brünger AT. 1998. Crystallography and NMR system: A new software suite for macromolecular structure determination. *Acta Crystallogr D54*:905–921.

Dougherty DA, Stauffer DA. 1990. Acetylcholine binding by a synthetic receptor: Implications for biological recognition. *Science 250*:1558–1560.

Dunwiddie CT, Neeper MP, Nutt EM, Waxman L, Smith DE, Hofmann KJ, Lumma PK, Garsky VM, Vlasuk GP. 1992. Site-directed analysis of the functional domains in the factor Xa inhibitor tick anticoagulant peptide. *Biochemistry 31*:12126–12131.

Higashi T. 1990. Auto-indexing of oscillation images. *J Appl Crystallogr 23*:252–257.

Jordan SP, Mao SS, Lewis SD, Shafer JA. 1992. Reaction pathways for inhibition of blood coagulation factor Xa by tick anticoagulant peptide. *Biochemistry 31*:5374–5380.

Laskowski RA, MacArthur MW, Moss DS, Thorton JM. 1993. PROCHECK: A program to check the stereochemical quality of protein structures. *J Appl Crystallogr 26*:283–291.

Lim-Wilby MSL, Hallenga K, de Maeyer M, Lasters I, Vlasuk GP, Brunck TK. 1995. NMR structure determination of tick anticoagulant peptide (TAP). *Protein Sci 4*:178–186.

Lin Z, Johnson ME. 1995. Proposed cation-π mediated binding by factor Xa. *FEBS Lett 370*:1–5.

Lubkowski J, Wlodawer A. 1999. Decamers observed in crystals of bovine pancreatic trypsin inhibitor. *Acta Crystallogr D55*:335–337.

Marquart M, Walter J, Deisenhofer J, Bode W, Huber R. 1983. The geometry of the reactive site and the peptide groups in trypsin, trypsinogen and its complexes with inhibitors. *Acta Crystallogr B39*:480–490.

Mochalkin I, Tulinsky A. 1999. Structures of thrombin retro-inhibited with SEL2711 and SEL2770 as they relate to factor Xa binding. *Acta Crystallogr D55*:785–793.

Navaza J. 1994. AMoRe: An automated package for molecular replacement. *Acta Crystallogr A50*:157–163.

Nicholls A, Sharp KA, Honig B. 1991. Protein folding and association: Insights from the interfacial and thermodynamic properties of hydrocarbons. *Proteins 11*:281–296.

Nienaber VL, Amparo EC. 1996. A noncleavable retro-binding peptide that spans the substrate binding cleft of serine proteases. *J Am Chem Soc 118*:6807–6810.

Rydel TJ, Tulinsky A, Bode W, Huber R. 1991. Refined structure of the hirudin–thrombin complex. *J Mol Biol 221*:583–601.

Schechter I, Berger A. 1967. On the size of the active site in proteases. *Biochem Biophys Res Commun 27*:157–162.

Schwabacher AW, Zhang S, Davy W. 1993. Directionality of the cation-π effect: A charge-mediated size selectivity in binding. *J Am Chem Soc 115*:6995–6996.

Tabernero L, Chang CY, Ohringer SL, Lau WF, Iwanowicz EJ, Han WC, Wang TC, Seiler SM, Roberts DGM, Sack JS. 1995. Structure of a retro-binding peptide inhibitor complexed with human α-thrombin. *J Mol Biol 246*:14–20.

van de Locht A, Stubbs MT, Bode W, Friedrich T, Bollschweiler C, Hoffken W, Huber R. 1996. The ornithodorin–thrombin crystal structure, a key to the TAP enigma? *EMBO J 15*:6011–6017.

Waxman L, Smith DE, Arcuri KE, Vlasuk GP. 1990. Tick anticoagulant peptide (TAP) is a novel inhibitor of blood coagulation factor Xa. *Science 248*:593–596.

Wei A, Alexander RS, Duke J, Ross H, Rosenfeld SA, Chang C. 1998. Unexpected binding mode of tick anticoagulant peptide complexed with bovine factor Xa. *J Mol Biol 283*:147–154.

Wlodawer A, Deisenhofer J, Huber R. 1987a. Comparison of two highly refined structures of bovine pancreatic trypsin inhibitor. *J Mol Biol 193*:145–156.

Wlodawer A, Nachman J, Gilliland GL, Gallagher W, Woodward C. 1987b. Structure of form III crystals of bovine pancreatic trypsin inhibitor. *J Mol Biol 198*:469–480.

Zhang E, Tulinsky A. 1997. The molecular environment of the Na^+ binding site of thrombin. *Biophys Chem 63*:185–200.